Arch Appl Mech (2013) 83:1239–1255
DOI 10.1007/s00419-013-0744-7

ORIGINAL

Fei Yan · Xia-Ting Feng · Peng-Zhi Pan · Yin-Ping Li

A continuous–discontinuous cellular automaton method for regular frictional contact problems

Received: 11 November 2012 / Accepted: 14 March 2013 / Published online: 27 March 2013

Abstract In the present paper, a continuous–discontinuous cellular automaton method is developed to model the discontinuous problems caused by regular frictional contact, in which level set method, discontinuous enriched shape function, discontinuous cellular automaton method and contact friction theory are combined, by which an analysis from continuity to discontinuity can be achieved, and no assembled stiffness matrix but only cell stiffness is needed in the whole calculation, because of the use of discontinuous cellular automaton method. In the present method, level set method is used to track the discontinuous surface, and discontinuous enriched shape function is employed to describe the discontinuity of displacement and stress. Contact friction theory is applied to construct the Coulomb frictional contact model of discontinuous surfaces; besides, combined with discontinuous cellular automaton method, a new mixed iteration method is proposed to obtain the solution of the problem, and no assembled stiffness matrix is constructed. And the frictional contact iterations are done simultaneously with the updating of cellular automaton, in which the contact states and contact areas can be previously obtained in the cellular automaton updating process, and the efficiency can get much higher. Finally, some numerical examples are given to show that the present method is effective and accurate and can be further extended into some practical engineering.

Keywords Continuous–discontinuous cellular automaton method · Frictional contact · Discontinuous cellular automaton · Mixed updating rule

1 Introduction

The numerical simulation of engineering frictional contact problems is one of the most difficult and demanding tasks in computational mechanics, and friction along sliding interfaces is a common occurrence in many engineering, such as rock crack propagation under compression-shear loading, metal forming operation, drilling pile and so on. However, frictional contact problems are highly nonlinear and require significant computer resources, which present two significant difficulties. Firstly, we generally do not know the contact regions of the interfaces, which depend on the loads, interface geometry, material, boundary conditions and so on. The interfacial surfaces can come into and go out of contact with each other, which are unpredictable. Besides, frictional sliding always occurs in most of contact problems, which are nonlinear and chaotic, makes the solution convergence difficult.

Frictional contact problems have been studied by a lot of experts in past few years, such as friction model, numerical method for simulating frictional contact motion and so on. Recently, Wiercigroch and Wojewoda [1–3] have done some important work about friction model, and they proposed a dry friction model and some numerical methods for solving those problems. For this work, we focus on static rock mechanics, so we

F. Yan (✉) · X.-T. Feng · P.-Z. Pan · Y.-P. Li
State Key Laboratory of Geomechanics and Geotechnical Engineering, Institute of Rock and Soil Mechanics, Chinese Academy of Science, 430071 Wuhan, China
E-mail: fyan@whrsm.ac.cn

use Coulomb model to reflect the contact motion of static rock crack interfaces; furthermore, some complex models, such as dry friction model by Wiercigroch and Wojewoda, will be applied for next researches.

With the development of mechanical science and its engineering applications, in addition to the increasing use of computer in mechanics, numerical methods like the finite element method (FEM) and more recently the meshless methods [4–6] have been the subjects of intensive researches for contact problem analysis. The frictional contact problems have been solved initially in the framework of FEM, and several contact searching algorithms have been developed. Hallquist et al. [7] proposed the master–slave contact algorithm and the single-surface contact algorithm; after that Zhong [8] developed the hierarchy territory contact algorithm, and Belytschko et al. [9] proposed the pinball contact algorithm.

Boundary element method (BEM) has been also applied widely in frictional contact problems, which was first applied to contact problems by Anderson [10] in 1980. After that, Mukherjee [11] and Kane [12] combined vectorial and parallel processing with boundary element method and applied for frictional contact problems. Then, elastoplasticity was combined with boundary element method and applied into contact problems [13].

In the framework of meshless method, the particle to particle contact algorithm and the penalty method were combined to apply for contact problems by Vignievic and Campbell et al. [14,15], and Li et al. [16] and Song et al. [17] proposed a meshfree contact detection algorithm, which was a completely meshfree contact-searching algorithm. Besides, some other contact algorithms used in meshless methods were extensions of the algorithms used in FEM [18].

The modeling of moving discontinuities with FEM is cumbersome, which is owing to the need to update the mesh topology to match the geometry of the discontinuity. So, the extended finite element method (XFEM) [19,20] developed rapidly, because this method circumvents these problems by enriching a standard mesh-based approximation with additional discontinuous functions. An algorithm that coupled the level set method with the extended finite element method was proposed by Stolarska et al. [21] and then applied for modeling linear elastic fracture. Recently, a numerical technique was developed by Sukumar et al. [22] for three-dimensional fatigue crack growth simulations. Besides, Xiao and Karihaloo [23] discussed the influence of quadrature rules on the accuracy of XFEM.

The XFEM was first applied into frictional contact problems by Dolbow et al. [24]. Later, Khoei et al. [25], Moes et al. [26] and Zi et al. [27] applied XFEM for cohesive crack growth, and Liu and Borja [28] proposed a new contact algorithm for frictional crack propagation, and compared the Newton–Raphson iteration and LATIN method. Elguedj et al. [29] developed a mixed augmented lagrangian XFEM for modeling elastoplastic fatigue crack growth with unilateral contact. Recently, Liu and Borja [30] proposed stabilized low-order finite elements for frictional contact with the extended finite element method.

Contact problems are always difficult to formulate and solve, because they usually involve inequality constraints. In order to deal with those problems, Curnier and Alart [31] proposed the penalty methods to circumvent the multivalued character. Furthermore, they introduced the augmented Lagrangian method to solve nonlinear programming problems [32], in which a mixed penalty-duality formulation for frictional contact problem was proposed, and then they also applied this method to solve discrete large-slip contact problems [33,34]. Later, Alart and Lebon [35] developed a multilevel interpolation adapted to the coarse/fine preconditioner and solved nonsymmetric and ill-conditioned linear systems.

Besides, a lot of numerical methods were developed to solve frictional contact problems. For example, Klarbring and Bjorkman [36] developed a mathematical programming approach to simulate frictional contact problems with varying contact surface, and Lebon and Raous [37] proposed a classical primal approach for piezoelectric materials, in which an implicit variational inequality was developed. Then, Chabrand et al. [38] developed finite elastoplastic strains to solve frictional contact problems. Later, two algorithms (FPM and GNM) had been described by Lebon [39] in order to numerically solve the contact problems, and a comparison between these two methods had been also given to illustrate the efficiency of those methods. In the present method, the penalty method is employed.

In order to accurately describe dynamic change from continuity to discontinuity in crack propagation process, Pan and Yan [40] combined level set method, enriched discontinuous shape functions and discontinuous cellular automaton method and proposed a new method, which was called as continuous–discontinuous cellular automaton method (CDCA), in which the calculation is focused on the cell only, and no assembled matrix is needed in the whole calculation.

Combining CDCA and the penalty method with Newton–Raphson method, CDCA can be extended into the application of frictional contact problems. In the present method, contact friction theory is applied to construct the contact friction model of discontinuous surfaces, in which the penalty method is combined with the CDCA. Besides, combined with discontinuous cellular automaton method and Newton–Raphson method,

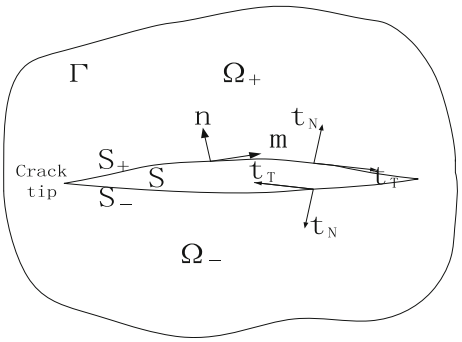

Fig. 1 Model of frictional contact problem

a mixed iteration method is proposed to obtain the solution of the problems, and no assembled stiffness matrix is constructed. With the help of updating rules of discontinuous cellular automaton method, the frictional contact iterations are done simultaneously with the updating of cellular automaton, in which the contact states and contact areas can be previously obtained in the cellular automaton updating, and the contact information and cell information can be updated simultaneously and then the efficiency can get much higher.

2 Frictional contact model and variational formulation

Consider a body Ω with a surface of discontinuity S, which is shown in Fig. 1. The discontinuity S includes two separate surfaces S_+ and S_-. According to contact theory, the surfaces S_+ and S_- are closed under the compression, and then a normal traction and a tangential friction force arise.

According to contact theory, the governing equations can be written as follows:

$$\operatorname{div}(\boldsymbol{\sigma}) + \mathbf{f} = \mathbf{0} \quad \text{in}\,\Omega \tag{1}$$

$$\mathbf{n} \cdot \boldsymbol{\sigma} = \mathbf{t} \quad \text{on}\,\Gamma_t \tag{2}$$

where $\boldsymbol{\sigma}$ is the stress tensor, $\mathbf{f}$ is the body force, $\mathbf{t}$ is traction vector acting on external surface Γ_t, $\mathbf{n}$ is normal vector of external surface. Besides, a discontinuous surface arises in the internal of the calculation domain, so the following conditions must be added:

$$\mathbf{n} \cdot \boldsymbol{\sigma} = \mathbf{t}_{S-} \quad \text{on}\ S_- \tag{3}$$

$$-\mathbf{n} \cdot \boldsymbol{\sigma} = \mathbf{t}_{S+} \quad \text{on}\ S_+ \tag{4}$$

According to the continuous–discontinuous cellular automaton theory [40] and XFEM theory [24,25], the displacement field $\mathbf{u}$ can be divided into continuous part $\bar{\mathbf{u}}$ and discontinuous part $\tilde{\mathbf{u}}$, which can be written as

$$\mathbf{u} = \bar{\mathbf{u}} + \tilde{\mathbf{u}} \tag{5}$$

The same as Eq. (5), we assume a weighting function, and its form is [24]

$$\boldsymbol{\eta} = \bar{\boldsymbol{\eta}} + \tilde{\boldsymbol{\eta}} \tag{6}$$

Then the standard variational formulation can be expressed as

$$\int_{\Omega} \nabla^S \boldsymbol{\eta} : \boldsymbol{\sigma} \mathrm{d}\Omega = \int_{\Omega} \boldsymbol{\eta} \cdot \mathbf{f} \mathrm{d}\Omega + \int_{\Gamma} \boldsymbol{\eta} \cdot \mathbf{t} \mathrm{d}\Gamma \tag{7}$$

Substituting the weighting function Eq. (6) into Eq. (10) yields

$$\int_{\Omega} \nabla^S (\bar{\boldsymbol{\eta}} + \tilde{\boldsymbol{\eta}}) : \boldsymbol{\sigma} \mathrm{d}\Omega + \int_{S} \tilde{\boldsymbol{\eta}} \cdot \mathbf{t}_{S-} \mathrm{d}\Gamma = \int_{\Omega} (\bar{\boldsymbol{\eta}} + \tilde{\boldsymbol{\eta}}) \cdot \mathbf{f} \mathrm{d}\Omega + \int_{\Gamma} (\bar{\boldsymbol{\eta}} + \tilde{\boldsymbol{\eta}}) \cdot \mathbf{t} \mathrm{d}\Gamma \tag{8}$$

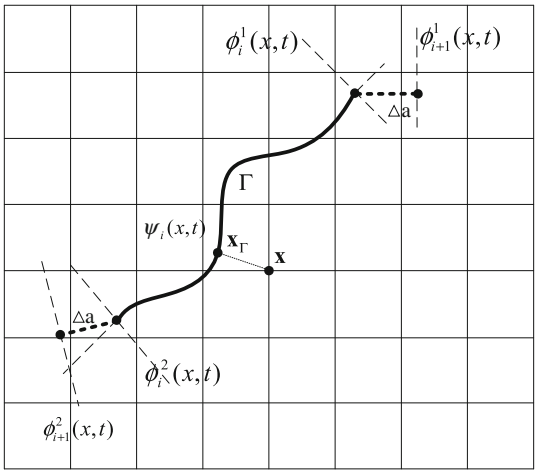

Fig. 2 Level set model

Since two weighting variables $\bar{\eta}$ and $\tilde{\eta}$ are independent, we can obtain two independent variational equations [24]

$$\int_\Omega \nabla^S \bar{\boldsymbol{\eta}} : \boldsymbol{\sigma} \mathrm{d}\Omega = \int_\Omega \bar{\boldsymbol{\eta}} \cdot \mathbf{f} \mathrm{d}\Omega + \int_\Gamma \bar{\boldsymbol{\eta}} \cdot \mathbf{t} \mathrm{d}\Gamma \tag{9}$$

$$\int_\Omega \nabla^S \tilde{\boldsymbol{\eta}} : \boldsymbol{\sigma} \mathrm{d}\Omega + \int_S \tilde{\boldsymbol{\eta}} \cdot \mathbf{t}_{S-} \mathrm{d}\Gamma = \int_\Omega \tilde{\boldsymbol{\eta}} \cdot \mathbf{f} \mathrm{d}\Omega + \int_\Gamma \tilde{\boldsymbol{\eta}} \cdot \mathbf{t} \mathrm{d}\Gamma \tag{10}$$

in which $\mathsf{T} = \int_S \tilde{\boldsymbol{\eta}} \cdot \mathbf{t}_{S-} \mathrm{d}\Gamma$ is a surface integral arising from contact on the surface of discontinuity. It can be seen that Eq. (9) is the standard FEM variational equation without a discontinuity, but Eq. (10) is the variational equation associated with the discontinuity, and it is noted that the region of integral for Eq. (10) is only carried out on the elements which are penetrated by the discontinuity.

3 Continuous–discontinuous cellular automaton method

3.1 Contact interface tracking

A powerful tool for tracking moving interface is the level set method, which is first introduced by Osher et al. [41], and the present method can benefit greatly by this method, which is based on the idea of representing the moving interface as a zero level set curve of a higher-dimensional function $\varphi(\mathbf{x}, t)$. Then, the evolution of the moving interface can be expressed as an evolution of equation $\varphi(\mathbf{x}, t)$.

In general, a discontinuous surface $\gamma(t) \subset R^2$ can be expressed as the level set curve of a function $\varphi(\mathbf{x}, t) = 0$ [42,43], which is shown in Fig. 2, and the expression can be given as

$$\gamma(t) = \left\{ \mathbf{x} \in R^2 : \varphi(\mathbf{x}, t) = 0 \right\} \tag{11}$$

Then the level set function $\varphi(\mathbf{x}, t)$ would be the signed distance function, which is

$$\varphi(\mathbf{x}, t) = \xi(\mathbf{x}, t) = \min_{\mathbf{x}_\Gamma \in \Gamma(t)} \|\mathbf{x} - \mathbf{x}_\Gamma\| \cdot \mathrm{sign}(\mathbf{n}^+ \cdot (\mathbf{x} - \mathbf{x}_\Gamma)) \tag{12}$$

in which $\mathbf{x}$ is the point outside of the crack surface and $\mathbf{x}_\Gamma$ is any point nearest to point $\mathbf{x}$ on the crack surface; $\mathbf{n}^+$ is a unit normal to the crack surface.

Discretization of level set allows for the evaluation of the level set function at the element level based on the nodal level set values $\varphi_j = \varphi_j(\mathbf{x}_j, t)$ and known classical finite element shape functions $N_j(\mathbf{x})$ [42,43],

$$\varphi(\mathbf{x}, t) = \sum_{j=1}^{n} N_j(\mathbf{x}, t) \varphi_j \tag{13}$$

This is practically an important concept for implicitly defining the level set function for describing a general moving interface. This simple procedure of defining the level set function can be widely used in some other methods. Another major advantage of this approximation is that the derivatives of the level set function can be obtained by the classical finite element shape functions,

$$\varphi_{,i}(\mathbf{x},t)=\sum_{j=1}^{n}N_{j,i}(\mathbf{x},t)\varphi_j \tag{14}$$

Only level set function of $\varphi(\mathbf{x},t)$ is not generally sufficient to describe a moving crack, so another level set function at the crack tip $\phi^i(\mathbf{x},t)$ is defined. The crack tip is represented as the intersection of the zero-level set function of $\varphi(\mathbf{x},t)$ with another zero-level set function of $\phi^i(\mathbf{x},t)$, where i is the number of tips on a given crack. So the crack tip level set function $\phi^i(\mathbf{x},t)$ is generally assumed to be orthogonal to $\varphi(\mathbf{x},t)$ [42,43]

$$\nabla\varphi(\mathbf{x},t)\nabla\phi(\mathbf{x},t)=0 \tag{15}$$

The same as Eq. (13), the level set function $\phi^i(\mathbf{x},t)$ can also be interpolated over the mesh by the same finite element shape functions,

$$\phi^i(\mathbf{x},t)=\sum_{j=1}^{n}N_j(\mathbf{x})\phi_j^i(\mathbf{x}_j,t) \tag{16}$$

The values of level set functions are stored only at nodes, and the values of all other points can be interpolated from their node values. For memory saving, only values of related part of nodes are calculated and stored. Moving crack is modeled by appropriately updating the functions of $\phi^i(\mathbf{x},t)$ and $\varphi(\mathbf{x},t)$, and the calculation grid is not changed in all over the calculation.

3.2 Self-contact constitutive model

Considering the contact motion of static rock interfaces, we use a simple contact model to describe according to reference [1,3], so the Coulomb friction model is employed, such as

$$F_c(\mathbf{P}_\mathrm{N},\mathbf{u})=\|\mathbf{P}_\mathbf{T}\|-\mu_C(\mathbf{P}_\mathbf{N},\mathbf{u})\,\|\mathbf{P}_\mathbf{N}\|-C_c\begin{cases}=0 & \text{slip}\\ <0 & \text{stick}\end{cases} \tag{17}$$

In the present method, the discontinuous surface S could cut through the interior of the finite element, so the contact model in this method is actually a self-contact kinematics. In self-contact model, the constitutive law on discontinuous surface should be formulated in the interior of the element rather than the nodes and sides of different elements of the classical FEM. The gap function of discontinuous surface is given as

$$g_N(x)=[\mathbf{u}_+(\mathbf{x})-\mathbf{u}_-(\mathbf{x})]\cdot\mathbf{n}(\mathbf{x})=\tilde{\mathbf{u}}(\mathbf{x})\cdot\mathbf{n}(\mathbf{x}) \tag{18}$$

where $\mathbf{u}_+(\mathbf{x})$ and $\mathbf{u}_-(\mathbf{x})$ are the displacements at $\mathbf{x}$ interpreted to lie on the Ω_+ and Ω_- sides of discontinuous surface S, respectively. And the relative tangential displacement vector can be given as

$$g_T(x)=[\mathbf{u}_+(\mathbf{x})-\mathbf{u}_-(\mathbf{x})]\cdot\mathbf{m}(\mathbf{x})=\tilde{\mathbf{u}}(\mathbf{x})\cdot\mathbf{m}(\mathbf{x}) \tag{19}$$

In the normal direction, contact condition on the discontinuous surface S can be expressed as

$$g_N\geq 0,\quad t_N\leq 0,\quad g_N t_N=0 \tag{20}$$

in which the component of traction $t_N=\mathbf{t}_{S-}\cdot\mathbf{n}$ represents the contact pressure, which satisfies the gap condition if $g_N>0$, then $t_N=0$, and the contact condition if $g_N=0$, then $t_N<0$.

In the tangential direction, we distinguish between stick and slip conditions, which are governed by a frictional constitutive law; then, the tangential traction t_T on the S can be written as

$$t_T=\mathbf{t}_{S-}\cdot\mathbf{m}\quad f=t_T+\mu t_N\leq 0 \tag{21}$$

In this paper, we impose a contact condition through the penalty method. For the normal component, we replace t_N by the constitutive expression

$$t_N = \varepsilon_N g_N \tag{22}$$

where ε_N is a normal penalty parameter analogous to a normal spring that allows the contact surfaces to slightly overlap. For the tangential component, a predictor–corrector scheme which mimics the classical plasticity theory is constructed. Assume that $(\mathbf{t_T})_n$ is the tangential friction of n iteration step and $\Delta\mathbf{g_T}$ is the increment in relative displacement of discontinuous surface in tangential direction. So the traction predictor can be written as [24]

$$\mathbf{t_T^{tr}} = (\mathbf{t_T})_n + \varepsilon_T \Delta\mathbf{g_T} \tag{23}$$

Check whether $\mathbf{t_T^{tr}} + \mu\varepsilon_N g_N \leq 0$, if so, we accept the predictor as the final value, in which contact condition is stick; otherwise, we use the backward implicit algorithm to correct for plastic sliding, in which the contact condition is slip. So we can get the tangential traction by a return mapping algorithm, which is given as [24]

$$\begin{cases} (\mathbf{t_T})_{n+1} = (\mathbf{t_T})_n + \varepsilon_T \Delta\mathbf{g_T} & \mathbf{t_T^{tr}} + \mu\varepsilon_N g_N \leq 0 \\ (\mathbf{t_T})_{n+1} = -\mu\varepsilon_N g_N \dfrac{\mathbf{t_T^{tr}}}{\|\mathbf{t_T^{tr}}\|} & \mathbf{t_T^{tr}} + \mu\varepsilon_N g_N > 0 \end{cases} \tag{24}$$

The iteration finishes when unbalanced force is equal to zero.

3.3 Discontinuous cellular automaton model

It is known to us that the displacements of the nodes of upper and bottom surface of crack are different; in order to model the strong discontinuity caused by the crack, the signed function is chosen as the Heaviside enrichment function; besides, a high-gradient stress field exists around the crack tip. So as to accurately model the crack tip stress field without element refinement, shape functions enriched by the exact near-tip asymptotic field functions are applied.

Then we can get the shape function of the present method, which can be given as

$$\mathbf{u}^h(\mathbf{x}) = \sum_{j=1}^{n} N_j(\mathbf{x})\mathbf{d}_j + \underbrace{\sum_{k=1}^{m} N_k(\mathbf{x})H(\xi)\mathbf{a}_k}_{k\in P} + \underbrace{\sum_{i=1}^{t} N_i(\mathbf{x}) \sum_{l=1}^{\mathrm{nf}} F_l(\mathbf{x})\mathbf{b}_i^l}_{i\in T} \tag{25}$$

in which n and m are the node numbers of element, P is the penetrated node set, $\mathbf{d}_j$ is the regular displacement vector, $\mathbf{a}_{jk}$ is a vector of additional degrees of nodal freedoms for modeling strong discontinuity, t is node number associated with crack tip, and T is crack tip node set, which can be seen in Fig. 1; nf is the number of the exact near-tip asymptotic field functions; $\mathbf{b}_i^l$ is a vector of additional degrees of nodal freedoms for modeling crack tip stress field, and $H(\xi)$ and $F_l(\mathbf{x})$ are Heaviside function and the exact near-tip asymptotic field functions, respectively, which are given as

$$\{F_l(x), l = 1-4\} = \left\{\sqrt{r}\sin\left(\frac{\theta}{2}\right), \sqrt{r}\cos\left(\frac{\theta}{2}\right), \sqrt{r}\sin(\theta)\sin\left(\frac{\theta}{2}\right), \sqrt{r}\sin(\theta)\cos\left(\frac{\theta}{2}\right)\right\} \tag{26}$$

$$H(\xi) = \mathrm{sign}(\xi) = \begin{cases} 1 & \forall\xi > 0 \\ -1 & \forall\xi < 0 \end{cases} \tag{27}$$

in which r, θ can be seen in Fig. 3.

According to Eq. (5), we can see that the continuous part of the displacement field is

$$\bar{\mathbf{u}}(\mathbf{x}) = \sum_{j=1}^{n} N_j(\mathbf{x})\mathbf{d}_j \tag{28}$$

The discontinuous part of the displacement field is only limited to the nodes which belong to the penetrated elements and crack tip elements. Because $H(\xi) = 1$ and $\theta = \pi$ on discontinuous surface of S_+, and $H(\xi) = -1$

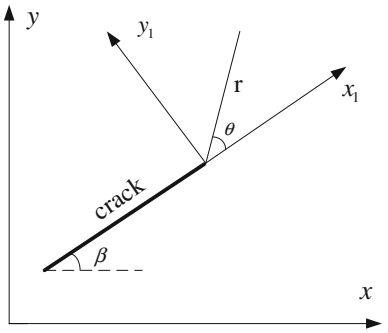

Fig. 3 Coordinate system of crack tip

and $\theta = -\pi$ on discontinuous surface of S_-, substitute those values into Eq. (25); we can get the discontinuous part of displacement field,

$$\tilde{\mathbf{u}}(\mathbf{x}) = 2\underbrace{\sum_{k=1}^{m} N_k(\mathbf{x})\mathbf{a}_k}_{k\in P} + 2\underbrace{\sum_{i=1}^{t} N_i(\mathbf{x})\sqrt{r}\mathbf{b}_i^0}_{i\in T} = \widehat{\mathbf{N}}\{\mathbf{a}\ \mathbf{b}\} \tag{29}$$

Substituting Eqs. (28) and (29) into Eqs. (9) and (10), we can get the residual equation [24]

$$\mathbf{r}(\mathsf{D}) = \begin{Bmatrix} \mathbf{F}_{\mathrm{EXT}} - \mathbf{F}_{\mathrm{INT}} \\ \mathsf{F}_{\mathrm{EXT}} - \mathsf{F}_{\mathrm{INT}} - \mathsf{T}_{\mathrm{INT}} \end{Bmatrix} \tag{30}$$

where $\mathsf{D} = \{\mathbf{d}\ \mathbf{a}\ \mathbf{b}\}^T$, $\mathbf{F}_{\mathrm{INT}}(\mathbf{d},\mathbf{a}) = \int_\Omega \mathbf{B}^{\mathbf{T}}\boldsymbol{\sigma}(\mathbf{d},\mathbf{a})\mathrm{d}\Omega$, $\mathbf{F}_{\mathrm{EXT}} = \int_\Omega \mathbf{N}^{\mathbf{T}}\mathbf{f}\mathrm{d}\Omega + \int_\Gamma \mathbf{N}^{\mathbf{T}}\mathbf{t}\mathrm{d}\Gamma$; $\mathsf{F}_{\mathrm{EXT}}(\mathbf{d},\mathbf{a},\mathbf{b}) = \int_{\Omega^h\setminus S} \tilde{\mathbf{B}}^{\mathbf{T}}\boldsymbol{\sigma}(\mathbf{d},\mathbf{a})\mathrm{d}\Omega$, $\mathsf{F}_{\mathrm{INT}} = \int_{\Omega^h} \tilde{\mathbf{N}}^{\mathbf{T}}\mathbf{f}\mathrm{d}\Omega + \int_{\Gamma^h} \tilde{\mathbf{N}}^{\mathbf{T}}\mathbf{t}\mathrm{d}\Gamma$, $\mathsf{T}_{\mathrm{INT}} = \int_S \widehat{\mathbf{N}}^{\mathbf{T}}\mathbf{t}_{S-}\mathrm{d}S$, in which $\tilde{\mathbf{N}}$ is the shape function matrix which is corresponding to Heaviside function enrichment and the exact near-tip asymptotic field function enrichment in Eq. (25) and $\tilde{\mathbf{B}}$ is derivative of shape function matrix. $\widehat{\mathbf{N}}$ is the shape function matrix corresponding to Eq. (29).

To solve this nonlinear problem, we iterate by Newton's method and cellular automaton updating rules. So we can get

$$\mathsf{D}_{n+1} = \mathsf{D}_n + \frac{r(\mathsf{D}_n)}{-r'(\mathsf{D}_n)} \tag{31}$$

in which the algorithmic tangent operator is

$$-\mathbf{r}'(\mathsf{D}_n) = \begin{bmatrix} \mathbf{A_{11}} & \mathbf{A_{12}} \\ \mathbf{A_{21}} & \mathbf{A_{22}} + \mathbf{C_{22}} \end{bmatrix} \tag{32}$$

in which stiffness matrices $\mathbf{A_{11}}$, $\mathbf{A_{12}}$, $\mathbf{A_{21}}$, $\mathbf{A_{22}}$ are common stiffnesses and the same as common continuous-discontinuous cellular automaton method, which can be seen in reference [40]. And $\mathbf{C}_{22}$ is the contact matrix, which is

$$\mathbf{C_{22}} = \int_{\mathbf{S}} \widehat{\mathbf{N}}^{\mathbf{T}}\mathbf{E}\widehat{\mathbf{N}}\mathrm{d}S \tag{33}$$

in which $\mathbf{E}$ is friction tangent matrix, and the problem is decomposed into a pure contact in the normal direction and frictional resistance in the tangential direction, which are linearized as

$$\mathbf{E} = \mathbf{T}^T \begin{bmatrix} G_f & 0 \\ 0 & E_f \end{bmatrix} \mathbf{T} \tag{34}$$

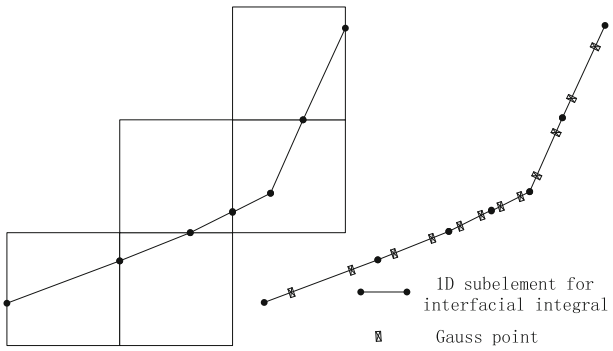

Fig. 4 Subelement and Gauss quadrature point of interfacial integral

in which $\mathbf{T}$ is the transformation matrix from global coordinate system to crack tip local crack coordinate system, G_f is the stick shear modulus of contact surface, and E_f is the normal stiffness, which can be chosen as an arbitrary large number for numerical convenience. And for the nodes of the penetrated elements,

$$\widehat{\mathbf{N}}_i = \begin{bmatrix} 0 & 0 & 2N_i & 0 \\ 0 & 0 & 0 & 2N_i \end{bmatrix} \tag{35}$$

And for the nodes which belong to crack tip elements,

$$\widehat{\mathbf{N}}_i = \begin{bmatrix} 0 & 0 & 2N_i\sqrt{r} & 0 & 0 & 0 & 0 & 0 & 0 & 0 \\ 0 & 0 & 0 & 2N_i\sqrt{r} & 0 & 0 & 0 & 0 & 0 & 0 \end{bmatrix} \tag{36}$$

in which N_i is the common shape function of classical FEM.

$\mathsf{T}_{\mathrm{INT}}$ in Eq. (30) and $\mathbf{C}_{22}$ in Eq. (32) are line integral, and the integral elements and gauss points can be seen in Fig. 4.

3.4 Updating rules of cellular automaton

Used discontinuous cellular automaton (DCA), the equilibrium state of the object can be obtained through the self-organization phenomenon formed by the one-another information transfer between cells. So the localization property of object can be easily treated, and the behavior of the cell is thought to be essentially local. There are three advantages for this theory. One is no need to assemble the overall matrix, especially for the enriched nodes, the degrees for some nodes may be different, which may bring some difficulties for the assembling operation. The second is that it is easy to consider the local properties of the cell, because the updating rule is only applying on the local cell. The third one is the easy implementation of parallel algorithm.

The DCA model is composed of cell, cell space, cell state, crack, neighborhood and updating rules and so on. Besides, DCA model includes the continuous cell and discontinuous cell. The updating rules are the most important part of the DCA model, because the updating rules will determine the stress state of a cell element [40,44].

According to Eq. (31), we can get

$$-r'(\mathsf{D}_n)\Delta\mathsf{D}_{n+1} = r(\mathsf{D}_n) \tag{37}$$

In one iteration step, we can assume that $\mathbf{K} = -r'(\mathsf{D}_n)$, $\Delta\mathbf{u} = \Delta\mathsf{D}_{n+1}$ and $\Delta\mathbf{f} = r(\mathsf{D}_n)$; based on this assumption, the discontinuous cellular automaton can be easily applied to solve this nonlinear system in this iteration step.

Considering a cellular node N_i for a plane elastic problem, the displacement of this node can be obtained due to the effect of nodal force vector $\mathbf{f}_i = \{\mathbf{f}_i^u, \mathbf{f}_i^a, \mathbf{f}_i^b\}$ and restrict all degrees of the nodal freedom on its neighbor cell nodes N_i^k, which can be shown in Fig. 5. The relation between the incremental force and incremental deformation can be reflected into two steps. Firstly, the nodal force increment $\Delta\mathbf{f}_i = \{\Delta\mathbf{f}_i^u, \Delta\mathbf{f}_i^a, \Delta\mathbf{f}_i^b\}$ will lead the cell node N_i to produce the displacement increment $\Delta\mathbf{u}_i^h = \{\Delta\mathbf{u}_i, \Delta\mathbf{a}_i, \Delta\mathbf{b}_i\}$. Then, the displacement

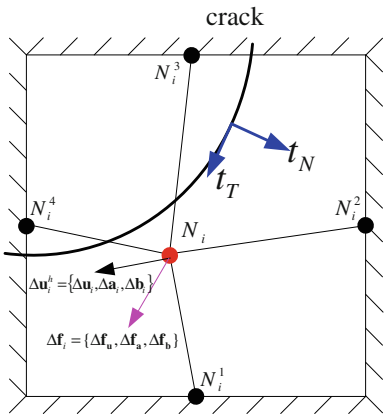

Fig. 5 Cell states and its updating model

increment $\Delta\mathbf{u}_i^h$ on the cell node N_i will lead its neighboring cell nodes to produce the nodal force increment $\Delta\mathbf{f}_i^k$.

Therefore, the process of the DCA updating rules is as follows: increment of nodal force leads to the increment of nodal displacement, and the increment of nodal displacement leads to the increment of nodal force of its neighboring nodes, until the system static equilibrium is achieved, in other words the self-organization phenomenon of $\Delta\mathbf{u}_i^h \to 0$ and $\Delta\mathbf{f}_i^k \to 0$ appears. So the updating steps can be given as:

(1) The equilibrium equation of the cell node N_i can be described as

$$\mathbf{K}_i \Delta\mathbf{u}_i^h = \Delta\mathbf{f}_i \tag{38}$$

in which $\mathbf{K}_i$ is the stiffness of cell node N_i, $\Delta\mathbf{u}_i^h = \{\Delta\mathbf{u}_i, \Delta\mathbf{a}_i, \Delta\mathbf{b}_i\}$, $\Delta\mathbf{f}_i = \{\Delta\mathbf{f}_i^u, \Delta\mathbf{f}_i^a, \Delta\mathbf{f}_i^b\}$ are increment of degrees of nodal freedom and nodal force, respectively, of cell node N_i.
Calculate the increment of degrees of nodal freedom $\Delta\mathbf{u}_i^h$ via the increment of nodal force $\Delta\mathbf{f}_i$.

(2) Restrict all degrees of nodal freedom on all neighboring cell N_i^k, which can be seen in Fig. 5.

(3) Obtain the nodal force increment $\Delta\mathbf{f}_i^k$ of the neighboring cell N_i^k via $\Delta\mathbf{u}_i^h$ from the following equation

$$\Delta\mathbf{f}_i^k = \mathbf{K}_i^k \Delta\mathbf{u}_i^h \tag{39}$$

where $\mathbf{K}_i^k$ is the stiffness of neighboring cell N_i^k.

(4) Finish the calculation of steps (1)–(3) on all cell nodes, until $\Delta\mathbf{u}_i^h \to 0$ and $\Delta\mathbf{f}_i^k \to 0$ appear.

4 Mixed iteration method

It can be seen that there are two iterations present in this method and they are Netwon–Raphson iteration for contact state iteration and information updating for discontinuous cellular automaton. In the present method, combined these two methods, a mixed iteration scheme is proposed, which may improve the calculation efficiency.

In last section, we can see that if the discontinuous cellular automaton updating is carried out separately in each Netwon–Raphson iteration, the calculation is time-consuming, therefore, a mixed iteration method, which the discontinuous cellular automaton updating and Netwon–Raphson iteration are conducted simultaneously. The present method needs no assembled global matrix, and the discontinuous cellular automaton updating is integrated into the nonlinear iteration, which can greatly improve the calculation efficiency. Combined with discontinuous cellular automaton updating, the mixed iteration can be given as

(1) Firstly, assuming that no contact is existed, get the nonlinear system function according to Eq. (37).

(2) Applying the boundary condition, do the discontinuous cellular automaton updating once; in other words, carry out updating scheme of Sect. 3.4 once.

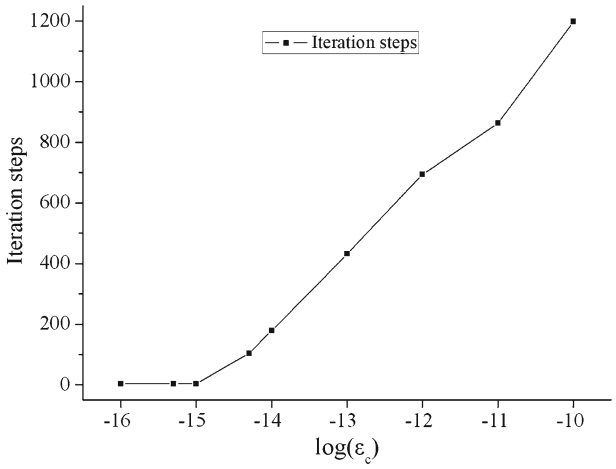

Fig. 6 Iteration steps of mixed iteration method

(3) Do step (2) for all cells one after another, updating the cell information, such as the stress, displacement and so on, until $\Delta \mathbf{u}_i^h \leq \varepsilon_c$.
(4) According to the preliminary results of step (3), calculate $g_N(x)$ and determine whether the contact state changes. If $g_N(x) \leq 0$, the contact occurs, and modify the cell stiffness matrix according to Eq. (33); otherwise, no contact occurs, and remove the contact stiffness from Eq. (33).
(5) According to the contact state analysis of step (4), get the contact force, update residual force according to Eq. (30) and get the nonlinear system of Eq. (37).
(6) Continue to do the discontinuous cellular automaton updating and Netwon–Raphson iteration of Step (2) to step (5), until $\Delta \mathbf{f} = r(\mathsf{D}_n) < \varepsilon_n$ appear, otherwise continue to do step (2) to step (5).
(7) Finish mixed iteration steps, and get the cell stresses, displacements and contact states and contact forces.

5 Numerical examples

In order to illustrate the accuracy and versatility of the present method in frictional contact problems, some numerical examples about contact frictional contact problems are investigated in this section.

5.1 Convergence study

A 0.1×0.1 thick plate is studied in this section, in which a horizontal uniform shear and a vertical uniform pressure are imposed on the top edge of the plate, and the bottom edge of the plate is constrained. Besides, a crack is located at the center of the plate, its starting coordinate is $(-0.02, -0.005)$, and its end coordinate is $(0.02, 0.005)$. And the Netwon–Raphson iteration residual is given as $\|r(\mathsf{D}_n)\|_2 < \varepsilon_n < 1.0\text{e}^{-4}$.

The iteration steps are shown in Fig. 6, which plots the iteration steps vary with the decrease in the iteration error ε_c of cellular automaton method. It can be seen in this figure that with a smaller iteration error, the global iteration steps decrease, but when $\varepsilon_c <= 1.0\text{e}{-}15$, this phenomenon is not very clear.

The CPU times with different iteration error ε_c are shown in Fig. 7, in which we can see that much larger or much less ε_c can cause much longer calculation time, and much appropriate value of ε_c is $1.0\text{e}{-}^{14}$.

5.2 Contact friction behavior of two elastic bodies

In this section, the continuous–discontinuous cellular automaton is employed to simulate the contact friction behavior between two slipping surfaces, which is shown in Fig. 8 [45]. The block is constrained at the bottom, while the uniform horizontal and vertical loadings of $p_x = 2.5 \times 10^3$ N/m and $p_y = 1 \times 10^4$ N/m are imposed at the top, and the Young's modulus and Poisson's coefficient are $E = 2 \times 10^{10}$ Pa and $\nu = 0.3$, respectively. The frictional coefficient of two elastic blocks is $\mu_f = 0.3$.

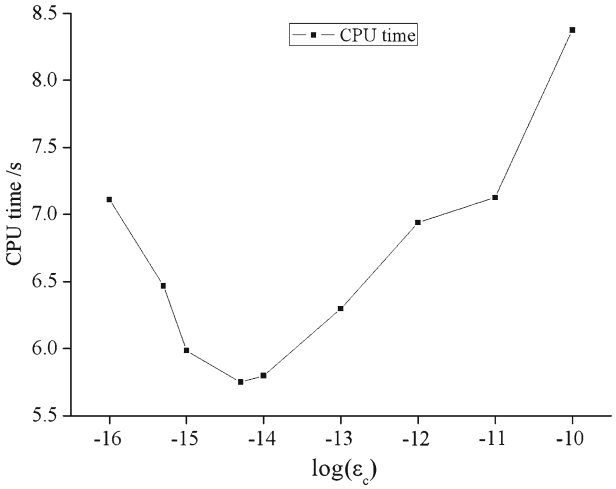

Fig. 7 CPU time of mixed iteration method

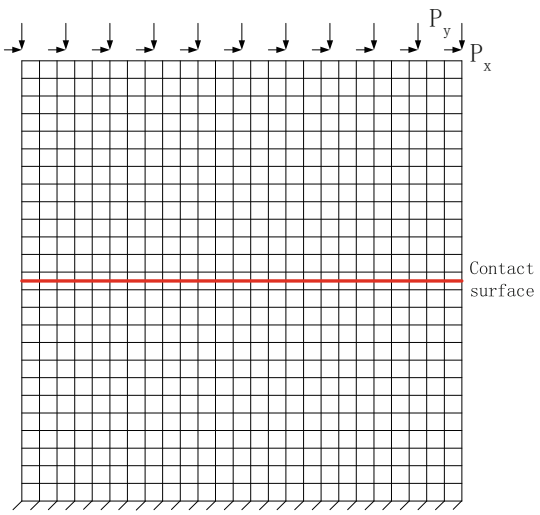

Fig. 8 Model of two sliding elastic bodies

In Figs. 9a, b, the distribution of shear stress of τ_{xy} contours at different shear modulus, i.e., $G_f = 1.0e11$ and $G_f = 1.0e8$ are presented. It can be seen that the results by the present method is very close to those of [45].

Besides, the normal compressive stress and tangential fiction with different coordinates are shown in Fig. 10; it is shown that if $x \leq 0.59$, sliding occurs, but $x > 0.59$, two elastic block are stick and no relative sliding occurs.

Figure 11 plots the computer memory comparison between CDCA and XFEM. It can be seen that much less computer memory is needed in CDCA than that of XFEM, which is very obvious when the element number gets much larger. Figure 12 shows the comparison of CPU time requirement between CDCA and XFEM, which is shown that the CPU time of XFEM decreases with the increasing of ε_n, and the smallest CPU time of CDCA is when ε_c is equal to $1.0e{-}14$, and at this case, the CPU times of those two methods are almost the same. But with CDCA, much less computer memory is needed, so the present method is much more efficient in all.

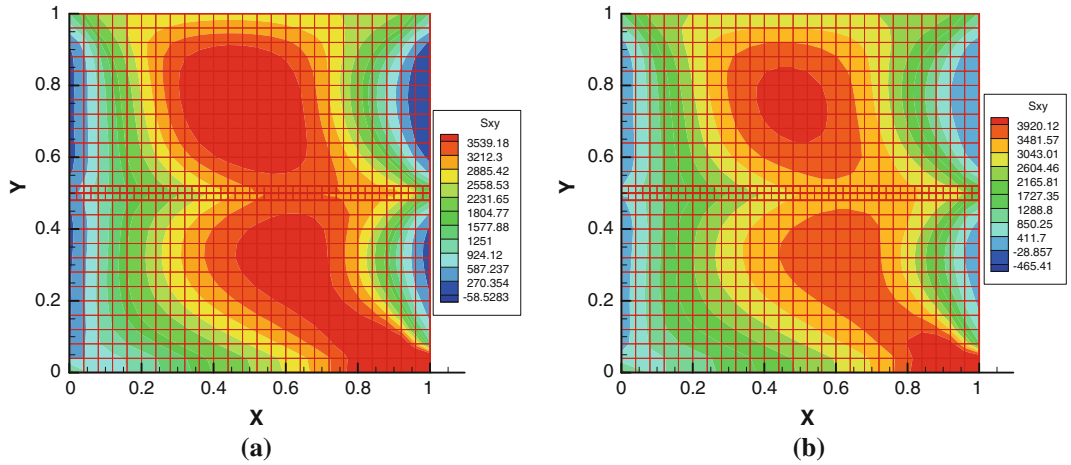

Fig. 9 Shear stress of τ_{xy} contours at different shear modulus. (**a**) Shear stress of $G_f = 1.0e11$. (**b**) Shear stress of $G_f = 1.0e8$

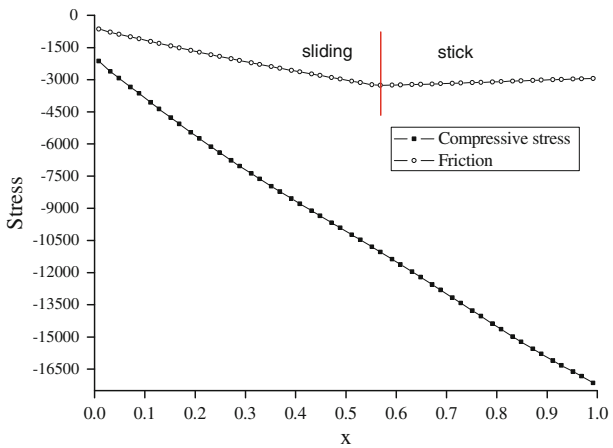

Fig. 10 Normal stress and tangential fiction of contact surface

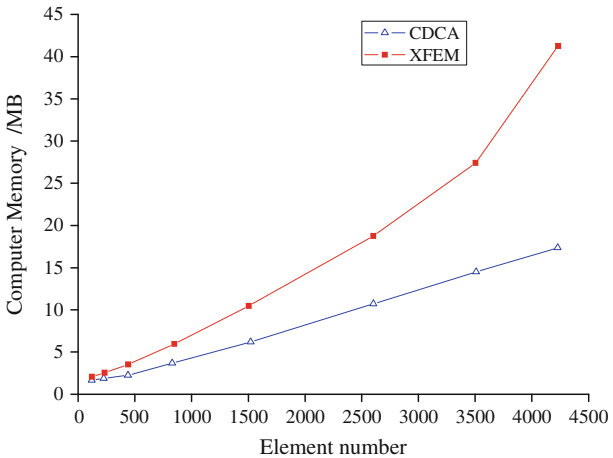

Fig. 11 Comparison for computer memory between different methods

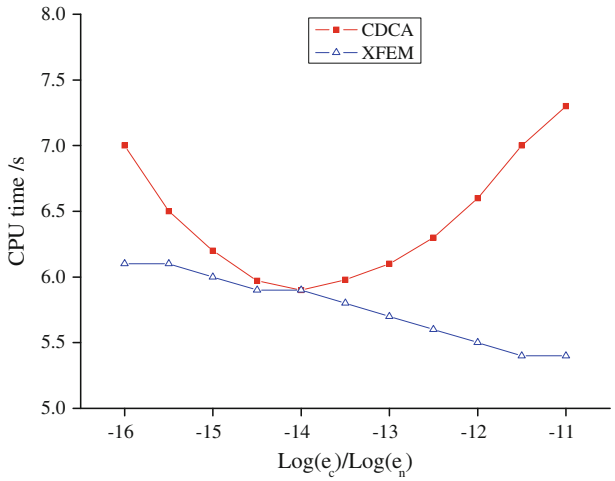

Fig. 12 Comparison for CPU time between different methods

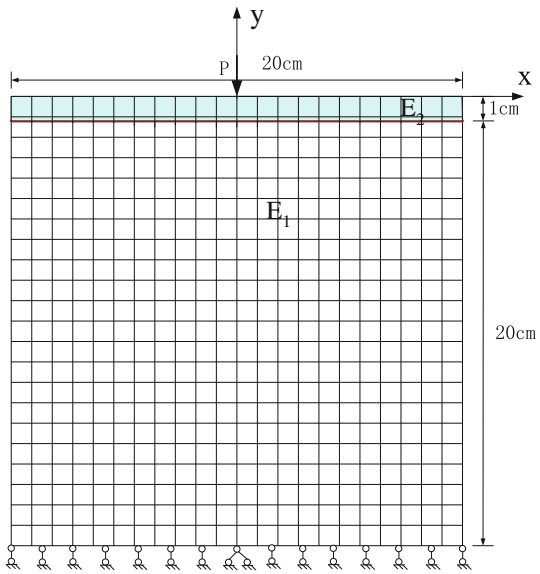

Fig. 13 Model and meshing of contact degradation problem

5.3 Contact degradation problem

A contact degradation problem is investigated in this section, in which the contact width becomes shorter when the loading is applied. It is shown in Fig. 13 that a lamellated plate is laid on a background; on the virtue of symmetry, only a half of the model is considered. In order to compare to the results of Keer [46], the parameters are given the same as Keer's. For lamellated plate, the elastic modulus $E_1 = 4$ GPa, $\nu_1 = 0.35$; for foundation basis, the elastic modulus $E_2 = 7.41228$ GPa, $\nu_2 = 0.35$, and different loadings p are applied on the center of the lamellated plate.

The convergence process of present example is plotted in Fig. 14, which is shown that it can converge quickly and smoothly by the present mixed iteration method. Besides, the contact pressures of contact surface between two blocks at $p = 5$ kN/m are shown in Fig. 15; it can be seen that the contact only occurs in $x < 12$ mm after the loading is imposed. In order to get much more results, different loadings are applied in this example, and the results are shown in Fig. 16, in which we can see that the contact areas are almost the same with different loadings, and those are very close to the results of Khoei [46] and Wang [47].

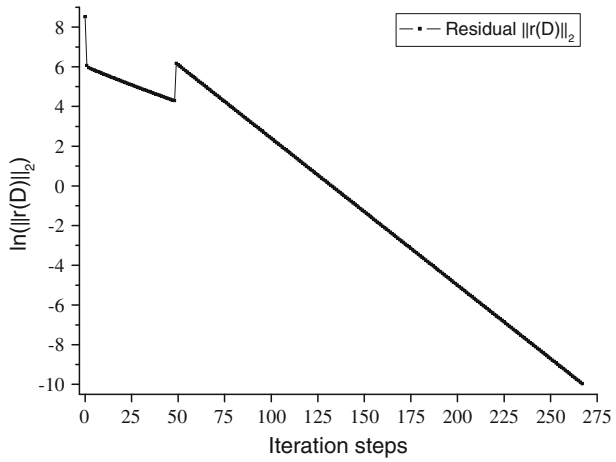

Fig. 14 Convergence process of present example

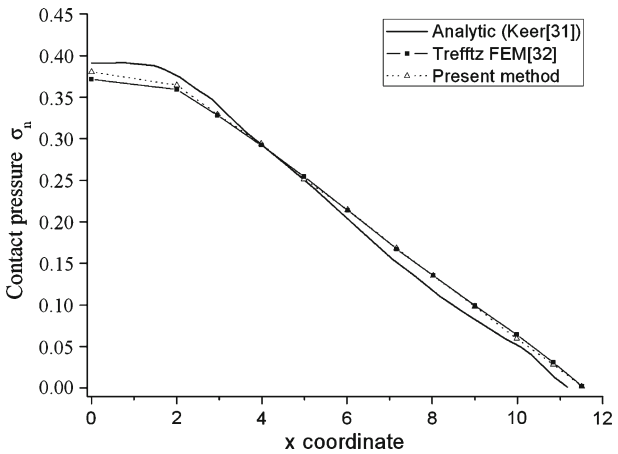

Fig. 15 Contact pressures at contact surface

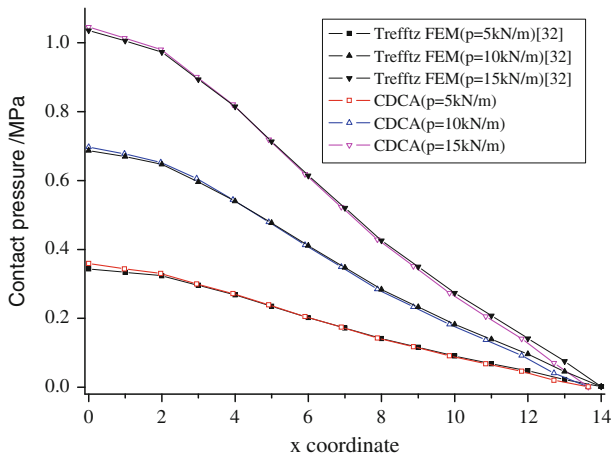

Fig. 16 Contact pressures at different loading

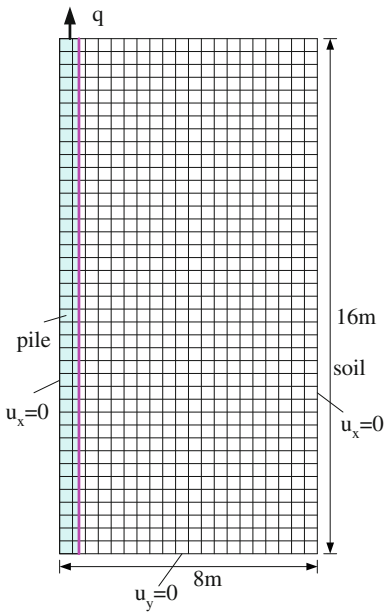

Fig. 17 model and meshing of the pile and soil

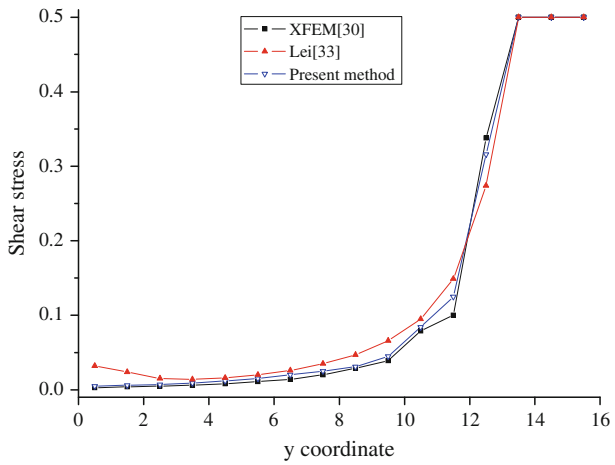

Fig. 18 Shear stress of contact surface between soil and pile

5.4 Pullout of pile

Pile foundations are widely used in highway construction, buildings and some other structures, so this example demonstrates the accuracy of the present method in pile foundation simulation. The model is shown in Fig. 17, and the results by Lei [48] are also given for compassion. The material properties of the concrete pile are as follows: $E_c = 2 \times 10^9$ Pa, $\nu_c = 0.3$ and density $\rho_c = 2.5 \times 10^3$ kg/m^3. The material properties of clay soil are given as: $E_s = 2 \times 10^8$ Pa, $\nu_c = 0.25$ and density $\rho_c = 2 \times 10^3$ kg/m^3. The contact friction behavior between pile and soil is modeled by the Mohr–Coulomb law with $c_f = 5$ kPa, $\mu_f = 0.58$ and the maximum tensile stress of $\sigma_s = 300$ kPa. The soil is restrained at the bottom and right-hand edges, and a tension force of $q = 50$ kN/m is imposed on the upper nodes of the pile. On the virtue of symmetry, the pile is analyzed for half of space, as shown in Fig. 15.

The shear stress along the contact surface due to the pullout force is presented in Fig. 18, which is compared with those obtained by Lei [48] and Khoei [45] using XFEM. It can be seen that a great agreement can be achieved between those three methods.

6 Conclusion

In the present paper, a method of continuous–discontinuous cellular automaton method (CDCA), which is based on level set method, the discontinuous enriched shape function, discontinuous cellular automaton method and contact friction theory, was developed for modeling frictional contact problems. Firstly, contact friction theory is applied to construct the contact friction model of discontinuous surfaces, in which the penalty method is combined with the CDCA. Besides, combined with discontinuous cellular automaton method and Newton–Raphson method, a mixed iteration method is proposed to obtain the solution of the problems, and no assembled stiffness matrix is constructed. And the frictional contact iterations are done simultaneously with the updating of cellular automaton, in which the contact states and contact areas can be previously obtained in the cellular automaton updating, and the contact information and cell information can be updated simultaneously and then the efficiency can get much higher.

Finally, numerical examples were presented to demonstrate the accuracy and capability of CDCA in modeling the frictional contact behavior. It is shown that the CDCA technology can be effectively used to modeling frictional contact problems.

Acknowledgements The wok was financially supported by the National key Basic Research Program of China (Nos. 2010CB732006, 2013CB036405), the National Natural Science Foundation of China (Nos. 11002154, 41272349 and 41172284) and the CAS/SAFEA International Partnership Program for Creative Research Teams (No. KZCX2-YW-T12).

References

1. Wojewoda, J.: Estimation of Lyapunov exponents for a system with sensitive friction model. Arch. Appl. Mech. **79**, 667–677 (2009)
2. Wojewoda, J., Stefanski, A., Wiercigroch, M., Kapitaniak, T.: Hysteretic effects of dry friction: modelling and experimental studies. Philos. Trans. R. Soc. A **366**, 747–765 (2008)
3. Stefanski, A., Wojewoda, J., Furmanik, K.: Experimental and numerical analysis of self-excited friction oscillator. Chaos Solitons Fractals **12**, 1691–1704 (2001)
4. Miao, Y., He, T.G., Yang, Q., Zheng, J.J.: Multi-domain hybrid boundary node method for evaluating top-down crack in asphalt pavements. Eng. Anal. Bound. Elem. **34**, 755–760 (2010)
5. Miao, Y., Wang, Q., Liao, B.H., Zheng, J.J.: A dual hybrid boundary node method for 2D elastodynamics problems. Comput. Model. Eng. Sci. **53**, 1–22 (2009)
6. Miao, Y., Wang, Y., Wang, Y.H.: A meshless hybrid boundary node method for helmholtz problems. Eng. Anal. Bound. Elem. **33**, 120–127 (2009)
7. Hallquist, J.O., Goudreau, G.L., Benson, D.J.: Sliding interfaces with contact-impact in large-scale lagrangian computation. Comput. Methods Appl. Mech. Eng. **51**, 107–137 (1985)
8. Zhong, Z.H.: Finite Element Procedures for Contact-Impact. Oxford university press, London (1993)
9. Belytschko, T., Yeh, I.S.: The splitting pinball method for contact-impact problems. Comput. Methods Appl. Mech. Eng. **105**, 375–393 (1993)
10. Anderson, T.: Boundary element method applied to two-dimensional contact problems with friction. Bound. Elem. Methods **211**(215), 211–215 (1981)
11. Zucchini, A., Mukherjee, S.: Vectorial and parallel processing in stress analysis with the boundary element method. Int. J. Numer. Methods. Eng. **31**, 307–317 (1991)
12. Kane, J.H.: Boundary element analysis on vector and parallel computers. Comput. Syst. Eng. **5**, 239–252 (1994)
13. Maier, G., Nappi, A., Novati, G.: Boundary element analysis in plasticity and mathematical programming. In: Du, Q.H. (eds.), Proceedings of the international conference on boundary elements. Pergamon Press, Oxford, pp. 261–273, (1986)
14. Vignjevic, R., Campbell, J.: A penalty approach for contact in smoothed particle hydrodynamics. Int. J. Impact Eng. **23**, 945–956 (1999)
15. Campbell, J., Vignjevic, R., Libersky, L.: A contact algorithm for smoothed particle hydrodynamics. Comput. Methods Appl. Mech. Eng. **184**, 49–65 (2000)
16. Li, S., Hao, W., Liu, W.K.: Numerical simulations of large deformation of thin shell structures using meshfree methods. Comput. Mech. **25**, 102–116 (2000)
17. Song, N., Qian, D., Cao, J., Liu, W.K., Li, S.: Effective models for prediction of springback in flanging. J. Eng. Mater. Tech. **123**, 456–461 (2001)
18. Chen, J.S., Wang, H.P.: New boundary condition treatments in meshfree computation of contact problems. Comput. Methods Appl. Mech. Eng. **187**, 441–468 (2000)
19. Belytschko, T., Black, T.: Elastic crack growth in finite elements with minimal remeshing. Int. J. Numer. Methods Eng. **45**, 601–620 (1999)
20. Moes, N., Dollow, J., Belytschko, T.: A finite element method for crack growth without remeshing. Int. J. Numer. Methods Eng. **46**, 131–150 (1999)
21. Stolarska, M., Chopp, D.L., Moes, N., Belytschko, T.: Modeling crack growth by level sets in the extended finite element method. Int. J. Numer. Methods Eng. **51**, 943–960 (2001)

22. Sukumar, N., Chopp, D.L., Moran, B.: Extended finite element method and fast marching method for three-dimensional fatigue crack propagation. Eng. Fract. Mech. **70**, 29–48 (2003)
23. Xiao, Q.Z., Karihaloo, B.L.: Improving the accuracy of XFEM crack tip fields using higher order quadrature and statically admissible stress recovery. Int. J. Numer. Methods Eng. **66**, 1378–1410 (2006)
24. Dolbow, J., Moes, N., Belytschko, T.: An extended finite element method for modeling crack growth with frictional contact. Comput. Methods Appl. Mech. Eng. **190**, 6825–6846 (2001)
25. Khoei, A.R., Nikbakht, M.: An enriched finite element algorithm for numerical computation of contact friction problems. Int. J. Mech. Sci. **49**, 183–199 (2007)
26. Moes, N., Belytschko, T.: Extended finite element method for cohesive crack growth. Eng. Fract. Mech. **69**, 813–833 (2002)
27. Zi, G., Belytschko, T.: New crack-tip elements for XFEM and applications to cohesive cracks. Int. J. Numer. Methods Eng. **57**, 2221–2240 (2003)
28. Liu, F.S., Borja, R.I.: A contact algorithm for frictional crack propagation with the extended finite element method. Int. J. Numer. Methods Eng. **76**, 1489–1512 (2008)
29. Elguedj, T., Gravouil, A., Combescure, A.: A mixed augmented Lagrangian-extended finite element method for modeling elastic-plastic fatigue crack growth with unilateral contact. Int. J. Numer. Methods Eng. **71**, 1569–1597 (2007)
30. Liu, F.S., Borja, R.I.: Stabilized low-order finite elements for frictional contact with the extended finite element method. Comput. Methods Appl. Mech. Eng. **199**, 2456–2471 (2010)
31. Curnier, A., Alart P.: A generalized Newton method for contact problem with friction. J. Mech. Theor. Appl. Special issue: Numerical Methods in Mechanics of Contact Involving Friction, 67–82 (1988)
32. Alart, P., Curnier, A.: A mixed formulation for frictional contact problems prone to Newton like solution methods. Comput. Methods Appl. Mech. Eng. **92**, 353–375 (1991)
33. Heegaard, J.H., Curnier, A.: An augmented lagrangian method for discrete large-slip contact problems. Int. J. Numer. Methods Eng. **36**, 569–593 (1993)
34. He, Q.C., Curnier, A.: Anisotropic dry friction between two orthotropic surfaces undergoing large displacements. Eur. J. Mech. A-Solids **12**, 631–666 (1993)
35. Alart, P., Lebon, F.: Solution of frictional contact problems using ILU and Coarse/fine preconditioners. Comput. Mech. **16**, 98–105 (1995)
36. Klarbring, A., Bjorkman, G.: A mathematical programming approach to contact problems with friction and varying contact surface. Comput. Struct. **30**, 1185–1198 (1988)
37. Lebon, F., Raous, M.: Friction modeling of a bolted junction under internal pressure loading. Comput. Struct. **43**, 925–933 (1992)
38. Chabrand, P., Dubois, F., Raous, M.: Various numerical methods for solving unilateral contact problems with friction. Math. Comput. Model. **28**, 97–108 (1998)
39. Lebon, F.: Contact problems with friction: models and simulations. Simul. Model. Practice Theory **11**, 449–463 (2003)
40. Pan, P.Z., Yan, F., Feng, X.T.: Modeling the cracking process of rocks from continuity to discontinuity using a cellular automaton. Comput. Geosci. **42**, 87–99 (2012)
41. Osher, S., Sethian, J.A.: Fronts propagating with curvature-dependent speed: algorithms based on Hamilton–Jacobi formulations. J. Comput. Phys. **79**, 12–49 (1988)
42. Sethian, J.: Evolution, implementation and application of level set and fast marching methods for advancing fronts. J. Comput. Phys. **19**, 503–555 (2001)
43. Stolarska, M., Chopp, D.L., Moes, N., Belytschko, T.: Modelling crack growth by level sets in the extended finite element method. Int. J. Numer. Methods Eng. **51**, 943–960 (2001)
44. Pan, P.Z., Feng, X.T., Houdson, J.A.: Study of failure and scale effects in rocks under uniaxial compression using 3D cellular automata. Int. J. Rock Mech. Min. Sci. **46**, 674–685 (2009)
45. Khoei, A.R., Nikbakht, M.: Contact friction modeling with the extended finite element method. J. Mater. Process. Technol. **177**, 58–62 (2006)
46. Keer, L.M., Dundurs, J., Tsai, K.C.: Problems involving a receding contact between a layer and a half space. J. Appl. Mech. **39**, 1115–1120 (1972)
47. Wang, K.Y., Qin, Q.H, Kang, Y.L. et al.: A direct constraint-Trefftz FEM for analyzing elastic contact problems. Int. J. Numer. Methods. Eng. **63**, 1694–1718 (2005)
48. Lei, X.: Contact friction analysis with a simple interface element. Comput. Methods Appl. Mech. Eng. **190**, 1955–1965 (2001)